Energy Conversion and Management 64 (2012) 113–121

Contents lists available at SciVerse ScienceDirect

Energy Conversion and Management

journal homepage: www.elsevier.com/locate/enconman

Comparison study on the battery models used for the energy management of batteries in electric vehicles

Hongwen He *, Rui Xiong, Hongqiang Guo, Shuchun Li

National Engineering Laboratory for Electric Vehicles, School of Mechanical Engineering, Beijing Institute of Technology, South No. 5 Zhongguancun Street, Beijing 100081, China

ARTICLE INFO

Article history:
Received 10 February 2012
Received in revised form 8 April 2012
Accepted 17 April 2012
Available online 24 September 2012

Keywords:
Battery models
Lithium-ion battery
Electric vehicles
Experiment
Battery management system

ABSTRACT

Battery model plays an important role in the simulation of electric vehicles (EVs) and states estimation of the batteries in the development of the model-based battery management system. To build a battery model with enough precision and suitable complexity, firstly this paper summarizes the seven representative battery models, which belong to the simplified electrochemical models or the equivalent circuit models. Then the model equations are built and the model parameters are identified with an online parameter identification method. The battery test bench is built and the experiment schedule is designed. Finally an evaluation is performed on the seven battery models by an experiment approach from the aspects of the estimation accuracy of the terminal voltages. To evaluate the effect of the number of RC networks on the model's precision, the battery general equivalent circuit models (GECMs) with different RC networks are also discussed further. The results indicate the equivalent circuit model with two RC networks, the *DP* model, has an optimal performance.

1. Introduction

Energy is the basis of the human survival and development, it's urgent to develop green energy and use the nonrenewable energy rationally. Since transportation consumes a large part of energy, to develop and apply the electric vehicles (EVs) is necessary in the way of green mobility [1–4]. Power battery is the key component of EVs, which include battery electric vehicles (BEVs), hybrid electric vehicles (HEVs) and plug-in hybrid electric vehicles (PHEVs). To ensure the power battery work safely and reliably, which is functioned by the battery management system (BMS) [5–7], the temperature, voltage, current of the batteries should be monitored and the states of the batteries should be estimated precisely in real time. However, it is hard to measure the states of batteries, like state of charge (SoC), state of health (SoH), state of function (SoF) directly for the complicated electrochemical process and various influence factors from the practice application, the estimation method based on battery models is used broadly and the battery model plays an important role [8–15].

Many battery models, which are lumped models with relatively few parameters, have been put forward especially for the purpose of vehicle power management control and battery management system development. The most commonly used models can be summarized as two kinds: the electrochemical models and the equivalent circuit models [9,15–21]. The electrochemical models utilize a set of coupled non-linear differential equations to describe the pertinent transport, thermodynamic, and kinetic phenomena occurring in the cell. They are relatively straight forward to translate the distributions into easily measurable quantities such as cell current and voltage, and build a relationship between the microscopic quantities, such as electrode and interfacial microstructure and the fundamental electrochemical studies and cell performance [22]. However, they typically deploy partial differential equations (PDEs) with a large number of unknown parameters, which often leads to a large memory requirement and a heavy computation burden, so the electrochemical battery models are not desirable for actual BMS (battery management system) [23] and the simplified electrochemical models, which ignore the thermodynamic and quantum effects, are proposed to simulate the electrochemical and voltage performance. The *Shepherd* model, the *Unnewehr Universal* model, the *Nernst* model and the *Combined* model are the typical representatives. The equivalent circuit battery models are developed by using resistors, capacitors and voltage sources to form a circuit network. Typically, a big capacitor or an ideal voltage source is selected to describe the open-circuit voltage (OCV), the remainder of the circuit simulates the battery's internal resistance and relaxation effects such as dynamic terminal voltage. The *Rint* model, the *Thevenin* model, the *DP* model and their revisions are widely used.

For the modeling and simulation of EVs and the development of the model-based BMS, the first important thing is to select and build a suitable battery model. How to evaluate and get a compromise in the balance of complexity and accuracy of the battery

* Corresponding author. Tel./fax: +86 10 6891 4842.
E-mail address: hwhebit@bit.edu.cn (H. He).

0196-8904/$ - see front matter © 2012 Elsevier Ltd. All rights reserved.
http://dx.doi.org/10.1016/j.enconman.2012.04.014

model is one of the key technologies, and also the problem to be discussed and solved in this paper.

2. Battery models and parameters identification method

2.1. The battery models

The equivalent circuits of the *Rint* model, the *Thevenin* model and the *DP* model are shown in Fig. 1. The equations and features of the seven representative battery models mentioned before are summarized and listed in Table 1.

Where U_t is the terminal voltage; K_0, K_1, K_2, K_3, K_4 are constants chosen to make the model fit the data well; I_L is the load current; R_o is the internal resistance; z_s is the abbreviation for SoC; U_{oc} is the open-circuit voltage; R_p is the equivalent polarization resistance and C_p is the equivalent polarization capacitance to model the battery relaxation effect during charging and discharging; U_p is the voltages across C_p; I_p is the outflow current of C_p; R_1, R_2 are the effective resistances and C_1, C_2 are the effective capacitances used to model the polarization characteristic in more details; U_1 and U_2 are the voltages across C_1 and C_2 respectively.

2.2. Model parameters' identification

The models' parameters identified by the traditional offline identification method maybe exit errors inevitably which caused by internal and external factors such as battery operating environment and aging, thus the accuracy will decrease. To solve these problems, we choose an online parameter identification method instead based on the recursive least squares (RLSs) method with an optimal forgetting factor.

2.2.1. The recursive least squares method with an optimal forgetting factor

A model-based method can provide a cheap alternative in estimation or it can be used along with a sensor-based scheme to provide some redundancy. The RLS method with an optimal forgetting factor (RLSF) has been widely used in estimation and tracking of time varying parameters in various fields of engineering. Many successful implementations of RLSF-based adaptive control for time varying parameters estimation are available in the literature [26–28].

We would like to apply the RLSF method in the prediction of battery terminal voltages with an online parameters' identification of the battery models. Consider a single input single output (SISO) process described by the general higher order auto-regressive exogenous (ARX) model:

$$y_k = \boldsymbol{\varphi}_k \boldsymbol{\theta}_k + \xi_k \tag{1}$$

where y is the system output, which denotes the terminal voltage U_t in this paper. $\boldsymbol{\varphi}$ and $\boldsymbol{\theta}$ are the information vector and the unknown parameter vector respectively. The parameters in $\boldsymbol{\theta}$ can either be constant or subject to infrequent jumps. ξ is a stochastic noise variable (random variable with normal distribution and zero mean), and k denotes the sample interval, $k = 0, 1, 2, \ldots$

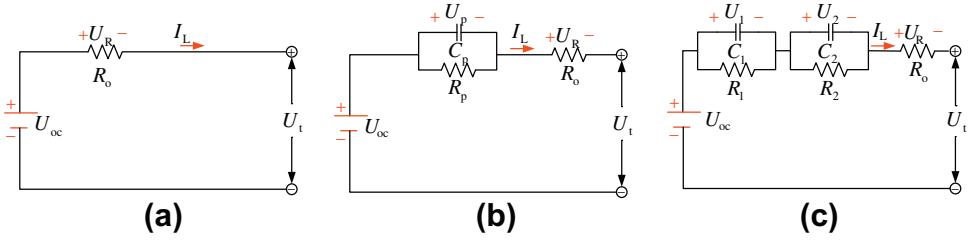

Fig. 1. Schematic diagram of equivalent battery circuit models: (a) The *Rint* model; (b) The *Thevenin* model; and (c) The *DP* model.

Table 1
Battery models and key features.

Classification	Models	Model equations and Features
Simplified electrochemical battery models [9]	1-*Shepherd* model	$U_t = K_0 - R_o I_L + K_1/z_s$ The model describes the electrochemical behavior of the battery directly in terms of voltage and current
	2-*Unnewehr Universal* Model	$U_t = K_0 - R_o I_L + K_2 z_s$ The model simplifies the *Shepherd* model and attempts to model the variation in resistance with respect to SoC
	3-*Nernst* model	$U_t = K_0 - R_o I_L + K_3 \ln z_s + K_4 \ln(1 - z_s)$ The model can be viewed as a modifications to the *Shepherd* model and uses exponential function with respect to SoC
	4-*Combined* model	$U_t = K_0 - R_o I_L + K_1/z_s + K_2 z_s + K_3 \ln z_s + K_4 \ln(1 - z_s)$ The model can be viewed as a combination of the previous three models to obtain the most accurate performance
Equivalent circuit battery models	5-*Rint* model [24]	$U_t = U_{oc} - I_L R_o$
	6-*Thevenin* model [25]	$\begin{cases} \dot{U}_p = \frac{I_L}{C_p} - \frac{U_p}{R_p C_p} \\ U_t = U_\infty - U_p - I_L R_o \end{cases}$ The model connects a parallel *RC* network in series based on the *Rint* model, describing the dynamic characteristics of the battery [25]
	7-*DP* model [21]	$\begin{cases} \dot{U}_1 = -\frac{U_1}{R_1 C_1} + \frac{I_L}{C_1} \\ \dot{U}_2 = -\frac{U_2}{R_2 C_2} + \frac{I_L}{C_2} \\ U_t = U_\infty - U_1 - U_2 - I_L R_o \end{cases}$ The model connects a parallel *RC* network in series based on the *Thevenin* model, in order to refine the description of polarization characteristics and simulate the concentration polarization and the electrochemical polarization separately which may leads to a more accurate performance

Then the system identification is realized as follows [28].

$$\begin{cases} \mathbf{K}_k = \frac{\mathbf{P}_{k-1}\boldsymbol{\varphi}_k^T}{\lambda+\boldsymbol{\varphi}_k^T\mathbf{P}_{k-1}\boldsymbol{\varphi}_k} \\ \mathbf{P}_k = \frac{\mathbf{P}_{k-1}-\mathbf{K}_k\boldsymbol{\varphi}_k^T\mathbf{P}_{k-1}}{\lambda} \\ e_k = y_k - \boldsymbol{\varphi}_k\hat{\boldsymbol{\theta}}_{k-1} \\ \hat{\boldsymbol{\theta}}_k = \hat{\boldsymbol{\theta}}_{k-1} + \mathbf{K}_k e_k \end{cases} \tag{2}$$

where $\hat{\boldsymbol{\theta}}_k$ is the estimate of the parameter vector $\boldsymbol{\theta}_k$; e_k is the prediction error of the terminal voltage; $\mathbf{K}_k$ is the algorithm gain and $\mathbf{P}_k$ is the covariance matrix; the constant λ is the forgetting factor, typically $\lambda \in [0.95, 1]$ and is very important to obtain a good estimated parameter set with small error.

2.2.2. Parameters' identification

The simplified electrochemical model in discrete form can be rewritten in the form of the ARX model, and then use the RLSF-based method to carry out parameter identification. While for the equivalent circuit model, there need to get a discrete form of the dynamic equations first, then use the RLSF-based method to carry out parameter identification.

Considering the bilinear transformation method can keep the dynamic characteristics of the system well, we adopt this method to discretize the dynamic equations.

The electrical behavior equation shown in Table 1 for the *Thevenin* model can be rewritten as follows in the frequency domain.

$$U_t(s) = U_{oc}(s) - I_L(s)\left(R_o + \frac{R_p}{1+R_pC_ps}\right) \tag{3}$$

Define $E_t = U_t - U_{oc}$, the transfer function $G(s)$ of Eq. (3) can be written as follows.

$$G(s) = \frac{E_t(s)}{I_L(s)} = -R_o - \frac{R_p}{1+R_pC_ps} = -\frac{R_o + R_p + R_oR_pC_ps}{1+R_pC_ps} \tag{4}$$

A bilinear transformation method shown in Eq. (5) is employed for the discretization calculation of Eq. (4) and the result is shown in Eq. (6).

$$s = \frac{2}{T_s}\frac{1-z^{-1}}{1+z^{-1}} \tag{5}$$

where z is the discretization operator and T_s is the sample interval. Herein, T_s is 1 s.

$$G(z^{-1}) = -\frac{a_2 + a_3z^{-1}}{1-a_1z^{-1}} \tag{6}$$

Define:

$$\begin{cases} a_1 = -\frac{1-2R_pC_p}{1+2R_pC_p} \\ a_2 = -\frac{R_o+R_p+2R_oR_pC_p}{1+2R_pC_p} \\ a_3 = -\frac{R_o+R_p-2R_oR_pC_p}{1+2R_pC_p} \end{cases} \tag{7}$$

Then the model parameters can be solved according to the united equations of a_1, a_2 and a_3. Ref. [11] concludes the model's parameters can be viewed as a constant value in limited sample intervals, then:

$$\dot{U}_{oc} \approx 0 \Rightarrow U_{oc,k} \approx U_{oc,k-1} \tag{8}$$

Similarly, the $\dot{R}_o \approx 0$ holds since the sampling period is relatively small, and then,

$$U_{t,k} = (1-a_1)U_{oc,k} + a_1U_{t,k-1} + a_2I_{L,k} + a_3I_{L,k-1} \tag{9}$$

Similarly, the *DP* model can be discretized with the bilinear method, and then:

Table 2
The detailed recursive equations of the battery models.

Battery models	Recursion equations
1-*Shepherd* model	$\begin{cases} y_k = U_{t,k} \\ \boldsymbol{\varphi}_{1,k} = [1 \quad -I_{L,k} \quad 1/z_{s,k}] \\ \boldsymbol{\theta}_{1,k} = [E_{0,k} \quad R_{o,k} \quad K_{1,k}]^T \end{cases}$
2-*Unnewehr Universal* Model	$\begin{cases} y_k = U_{t,k} \\ \boldsymbol{\varphi}_{2,k} = [1 \quad -I_{L,k} \quad 1/z_{s,k}] \\ \boldsymbol{\theta}_{2,k} = [E_{0,k} \quad R_{o,k} \quad K_{2,k}]^T \end{cases}$
3-*Nernst* model	$\begin{cases} y_k = U_{t,k} \\ \boldsymbol{\varphi}_{3,k} = [1 \quad -I_{L,k} \quad \ln z_{s,k} \quad \ln(1-z_{s,k})] \\ \boldsymbol{\theta}_{3,k} = [E_{0,k} \quad R_{o,k} \quad K_{3,k} \quad K_{4,k}]^T \end{cases}$
4-*Combined* model	$\begin{cases} y_k = U_{t,k} \\ \boldsymbol{\varphi}_{4,k} = [1 \quad -I_{L,k} \quad 1/z_{s,k} \quad z_{s,k} \quad \ln z_{s,k} \quad \ln(1-z_{s,k})] \\ \boldsymbol{\theta}_{4,k} = [E_{0,k} \quad R_{o,k} \quad K_{1,k} \quad K_{2,k} \quad K_{3,k} \quad K_{4,k}]^T \end{cases}$
5- *Rint* model	$\begin{cases} y_k = U_{t,k} \\ \boldsymbol{\varphi}_{5,k} = [1 \quad I_{L,k}] \\ \boldsymbol{\theta}_{5,k} = [U_{oc,k} \quad -R_{o,k}]^T \end{cases}$
6-*Thevenin* model	$\begin{cases} y_k = U_{t,k} \\ \boldsymbol{\varphi}_{6,k} = [1 \quad U_{t,k-1} \quad I_{L,k} \quad I_{L,k-1}] \\ \boldsymbol{\theta}_{6,k} = [(1-a_1) \quad U_{oc,k} \quad a_1 \quad a_2 \quad a_3]^T \end{cases}$
7-*DP* model	$\begin{cases} y_k = U_{t,k} \\ \boldsymbol{\varphi}_{7,k-1} = [1 \quad U_{t,k-1} \quad U_{t,k-2} \quad I_{L,k} \quad I_{L,k-1} \quad I_{L,k-2}] \\ \boldsymbol{\theta}_{7,k} = [(1-b_1-b_2) \quad U_{oc,k} \quad b_1 \quad b_2 \quad b_3 \quad b_4 \quad b_5]^T \end{cases}$

$$U_{t,k} = (1-b_1-b_2)U_{oc,k} + b_1U_{t,k-1} + b_2U_{t,k-2} + b_3I_{L,k} + b_4I_{L,k-1} + b_5I_{L,k-2} \tag{10}$$

where b_1, b_2, b_3, b_4 and b_5 are the coefficient which contain model's parameters, and the detailed recursion solution equations for the above seven models are listed in Table 2.

Where $\boldsymbol{\varphi}_{i,k}$ is the information matrix and $\boldsymbol{\theta}_{i,k}$ is the unknown parameter matrix of the ith model, $i = 1, 2, 3, \ldots, 7$.

3. Experiments and data sampling

In order to sample the measurement data from the sensors to perform the model parameters' identification and the performance evaluation on the battery models, the battery test bench is built and the experiment schedule is designed.

3.1. Battery test bench

The test bench is shown in Fig. 2, which consists of a Digatron battery test system BNT 400-050, a thermal chamber for environment control, a host computer and BTS-600 interface for programming the BNT 400-050. The host computer is used for the real-time calculation of the model parameters. The BNT 400-050 can charge/discharge a battery according to the designed program with maximum voltage of 50 V and maximum charge/discharge current of 400 A, and its recorded data include current, voltage, temperature, accumulative amp–hours (A h) and watt–hours (W h), etc. The measured data is transmitted to the host computer through TCP/IP driven by BNT 400-050. The host computer has a low-pass filtering function to implement large noise cancellation [15]. Furthermore, in order to improve the sampling precision of cell voltage, the Fluke 8846A multimeter, whose measurement accuracy of DC voltage is up to 0.0024% with a 6.5 digit resolution, has been applied for cell voltage measurement [29]. A $LiFePO_4$ cell with nominal voltage of 3.2 V and nominal capacity of 10 A h is selected as the test object.

3.2. Battery test schedule

The battery is kept in the thermal chamber and the temperature is controlled within 20 ± 5 °C. The battery text schedule is designed

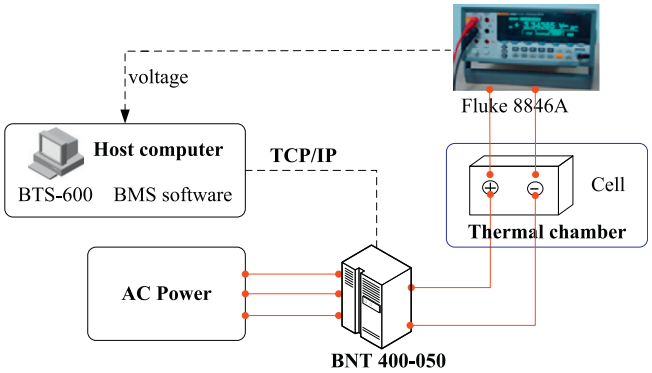

Fig. 2. The configuration of the battery test bench.

and shown in Fig. 3, which includes a characteristic test and an aging cycle test followed. For the characteristic test, the available capacity test is based on the standard of [30] to measure the maximum available capacity. Usually, the available capacity test is repeated three times. If the error of the experiment results between the maximum and the average is within 2%, the available capacity test is effective and the average value is taken as the actual maximum available capacity; however, if the error is more than 2%, the available capacity test should be repeated. The HPPC test is from the Battery Test Manual [31] and is the foundation of power battery characteristic test and parameter identification test, which achieves good results in off-line parameter identification and is used widely. The Dynamic Stress Test (DST) and the Federal Urban Dynamic Schedule (FUDS) test are the commonly used test procedures of Digatron [32]. The FUDS is a standard time-velocity profile for urban driving vehicles and has been widely used in the evaluation of model accuracy and SoC estimate of battery management system. For the driving-cycle testing of USABC batteries, a simplified version of the FUDS test is modified into the Dynamic Stress Test (DST). For the FUDS test, the DST test and the HPPC test, the battery SOC is controlled in the range of 0.25–1.0, 0.2–1.0 and 0–1.0 respectively.

3.3. Data of the battery experiment

In this paper, the data collected in the characteristic test of a fresh cell are arranged for the model parameters' identification and model evaluation.

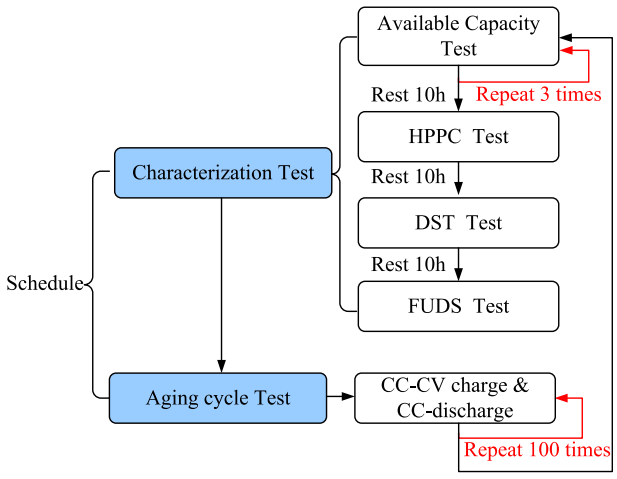

Fig. 3. Battery test schedules.

For the $LiFePO_4$ cell, the available capacity test shows that its actual maximum available capacity is 10.78 A h, slightly higher than 10 A h of the nominal capacity. The HPPC test results are shown in Fig. 4 including a sample HPPC current curve, a sample HPPC voltage curve under SoC = 0.8, the current profiles, the voltage profiles and the SoC profiles. The DST test results are shown in Fig. 5 including the current vs. time profiles and the SoC vs. time profiles. The FUDS test results are shown in Fig. 6 including the SoC profiles and one sample current profile of one FUDS cycle.

Due to the hard determination of the exact SoC value, here we determine the initial SoC and the terminal SoC of the $LiFePO_4$ lithium-ion battery according to the definition of SoC with a standard charging experiment and a further standard discharging experiment after finishing a test, so the initial SoC and the terminal SoC are accurate. The ampere–hour counting approach is used to calculate the SoC since it can keep track of the accurate SoC with an accurate initial SoC and a compensation of the coulombic efficiency. We also improve the SoC accuracy with a revision method based on the accurate terminal SoC. Considering all the battery experiments are carried out in a temperature chamber; the SoC calculation method is feasible with an acceptable accuracy.

4. Evaluation and discussion on the battery models

To evaluate the battery models rationally and objectively, an evaluation method is built first. Then the performances of the seven battery models are compared by the RLSF-based method. And the effect of the different RC networks of the equivalent circuit models are also discussed by a comparison of the terminal voltage estimation accuracy.

4.1. Evaluation method

To evaluate the battery models well, the online voltage estimation is performed with the HPPC test, the DST test and the FUDS test. Further, a statistics of the voltage error is analyzed in the aspects of the maximum, the minimum, the mean, the maximum of the RMSE (the root mean square error) and the mean of the RMSE. The voltage error denotes the difference between the experimental data and online estimated value. The RMSE denotes the deviation degree of the estimated value and the experimental value, which not only shows the present error, but also indicates the convergence of the estimation algorithm.

4.2. Evaluation analysis on the battery models

The evaluation results of the seven battery models under the HPPC test are shown in Fig. 7, including the statistics results of the voltage errors, the statistics results of the RMSE, the voltage profiles of model-based estimation with the representatives of the *Shepherd* model, the *Nernst* model, the *DP* model and the HPPC test. Fig. 7a shows that 6-*Thenenin* model and 7-*DP* model have smaller voltage errors, the mean of the voltage error of the simplified electrochemical models are also small. For 1-*Shepherd* model and 3-*Nernst* model, the maximum of voltage errors or the absolute value of the minimum of voltage errors are bigger than others. Fig. 7b shows that the RMSE of the seven models is less than 25 mV and is within 1% of the cell's nominal voltage, that means the online parameter identification method is effective. Just like the results of Fig. 7b, 6-*Thevenin* model and 7-*DP* model have smaller RMSE values and is better than the other five models under the HPPC test, since they takes the cell's relaxation effect into account for modeling. The fact, that 5-*Rint* model exists a big estimation error for the ignorance of the battery's dynamic voltage performance, indicates it is necessary to consider the voltage relaxation effect to

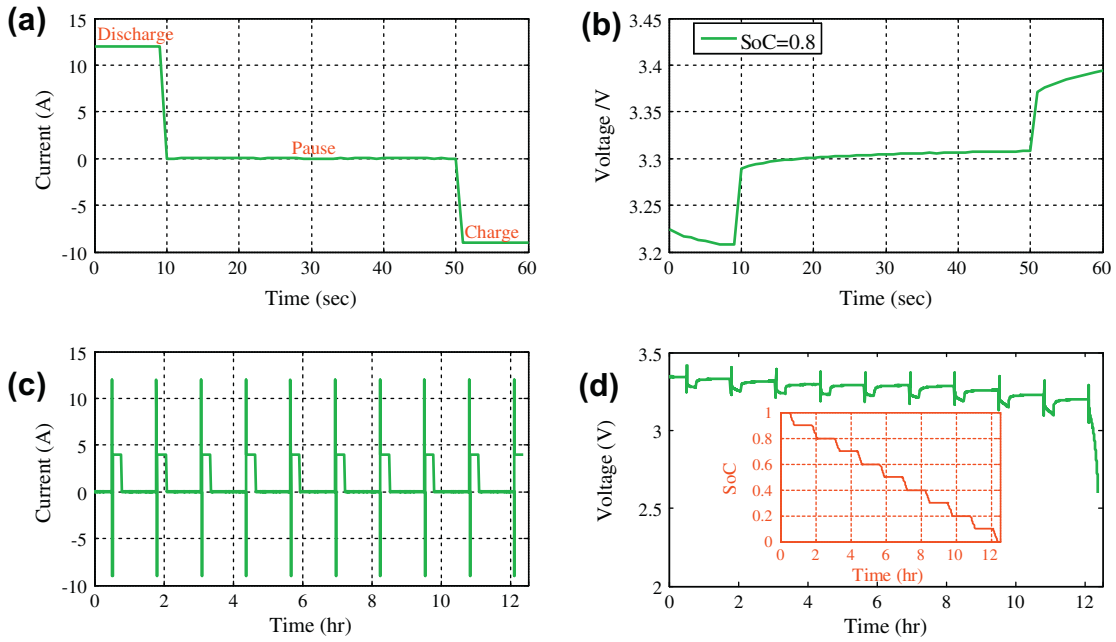

Fig. 4. The plots of the HPPC test: (a) the sample current vs. time profile of one HPPC; (b) the sample voltage vs. time profile of one HPPC; (c) the complete current vs. time profiles; and (d) the complete voltage vs. time profiles and the complete SoC vs. time profiles.

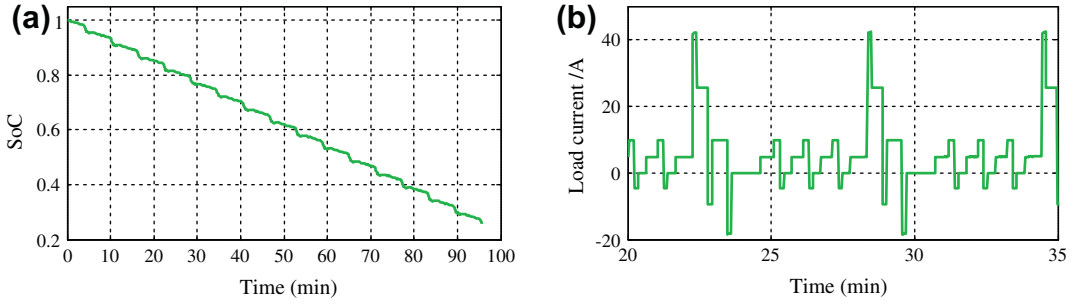

Fig. 5. The plots of the DST test: (a) the SoC vs. time profiles and (b) the current vs. time profiles.

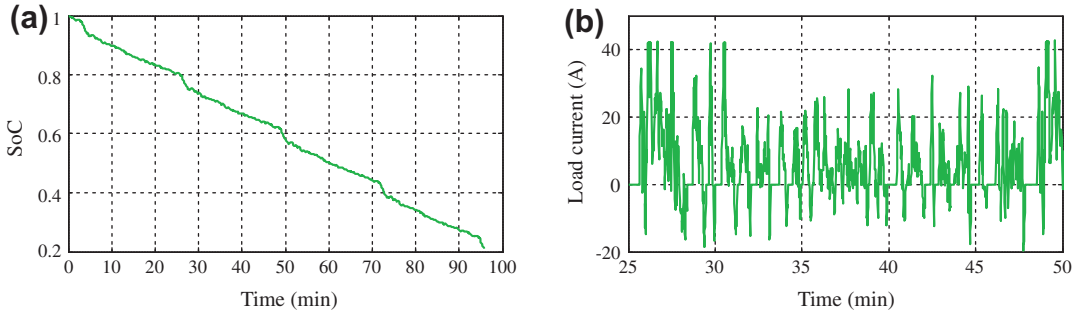

Fig. 6. The plots of the FUDS test: (a) the SoC vs. time profiles and (b) the sample current vs. time of one FUDS cycle.

improve the precision of the models for lithium-ion battery. Fig. 7c shows that the estimated voltages based on 1-*Shepherd* model nearly follow the test data except for the terminals where the SoC is nearly zero and the battery seldom works. Fig. 7b shows that 1-*Shepherd* model has higher precision than 3-*Nernst* model, that can also be verified from the fact, that the estimated voltage based on 3-*Nernst* model is higher than the experimental data at the end of the test and also a bigger voltage error of 3-*Nernst* model exists as shown in Fig. 7c. Fig. 7d shows that the terminal voltage estimated by 7-*DP* model agrees quite well with the experimental value. Based on the above analysis, it can be concluded that the *DP* model has the best dynamic voltage simulation performance among the seven battery models.

The evaluation results of the seven battery models under the *DST* test are shown in Fig. 8 including the statistics results of the voltage errors, the statistics results of the RMSE. Fig. 8a shows that 1-*Shepherd* model, 6-*Thevenin* model and 7-*DP* model have good online estimation precision with small voltage errors. Fig. 8b shows that 6-*Thevenin* model and 7-*DP* model have a relatively small RMSE, especially the 7-*DP* model. There can conclude that

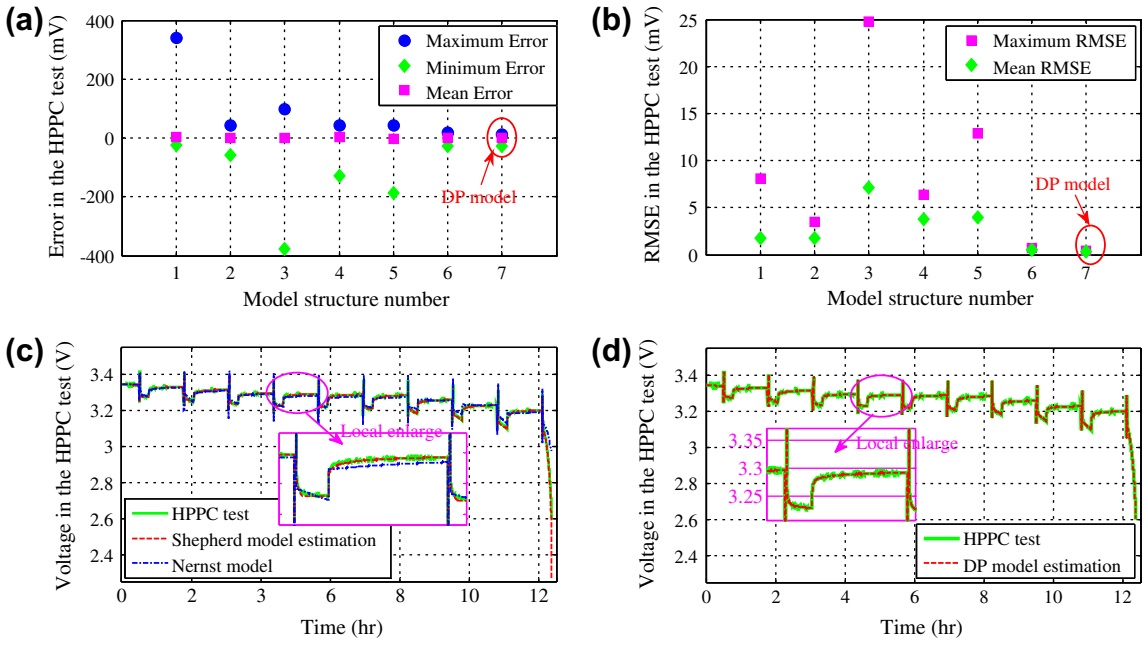

Fig. 7. Evaluation results under the HPPC test: (a) the statistics results of the voltage error; (b) the statistics results of the RMSE; (c) the voltage profiles of the *Shepherd* model-based estimation, the *Nernst* model-based estimation and the HPPC test; and (d) the voltage profiles of the *DP* model-based estimation and the HPPC test.

the *DP* model is the most outstanding model among the seven models, followed by 6-*Thevenin* model. This result agrees with the HPPC test. In Fig. 9, we choose two profiles in the DST test to describe the estimate accuracy between the estimated voltage by the *DP* model and the experiment data. It indicates that the *DP* model can simulate the battery's dynamic voltage performance very well under the DST test, which fully satisfies the development requirements of model-based BMS used in the EVs.

The evaluation results of the seven battery models under the FUDS test are shown in Fig. 10 including the statistics results of the voltage errors, the statistics results of the RMSE, the RMSE profiles of the four specific battery models, the voltage profiles of the *DP* model-based estimation and FUDS test data. Fig. 10a shows that the two models, 6-*Thevenin* model and 7-*DP* model, both of them take the polarization characteristics into consideration, have a smaller voltage error compared with other models. Also, Fig. 10b indicates that the mean of the RMSE of 6-*Thevenin* model and 7-*DP* model is the smallest. But the maximum of the RMSE of the *Thevenin* model is bigger than 1-*Shepherd* model and 2-*Unnewehr Universa*l model. Combined Fig. 10a and b, we can conclude that the *DP* model has a higher precision than other six models surely. However, to determine if 6-*Thevenin* is the second better model depends on the RMSE profile additionally. Fig. 10c intuitively indicates that 6-*Thevenin* model and 7-*DP* model restrain themselves

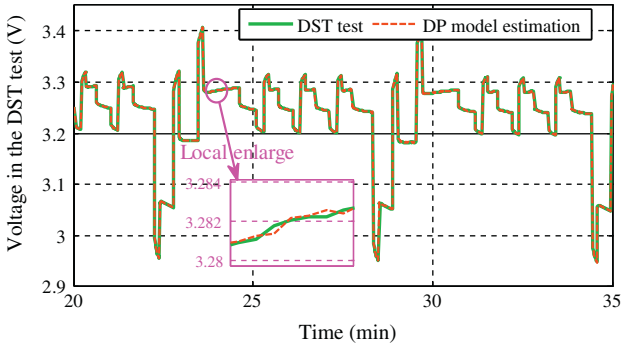

Fig. 9. The voltage profiles of the *DP* model-based estimation and the DST test data.

to approach the true values faster, so they have smaller mean of the RMSE, while 1-*Shepherd* model and 2-*Unnewehr Universal* model maintain themselves above 10 mV without a convergent tendency; The maximum of the RMSE of 6-*Thevenin* model is bigger than that of 1-*Shepherd* model and 2-*Unnewehr Universal* model. But for the convergent tendency, 6-*Thevenin* model is more stable, and the voltage error is less than 1-*Shepherd* model and 2-*Unnewehr Universal* model, so it can be determined that 6-*Thevenin*

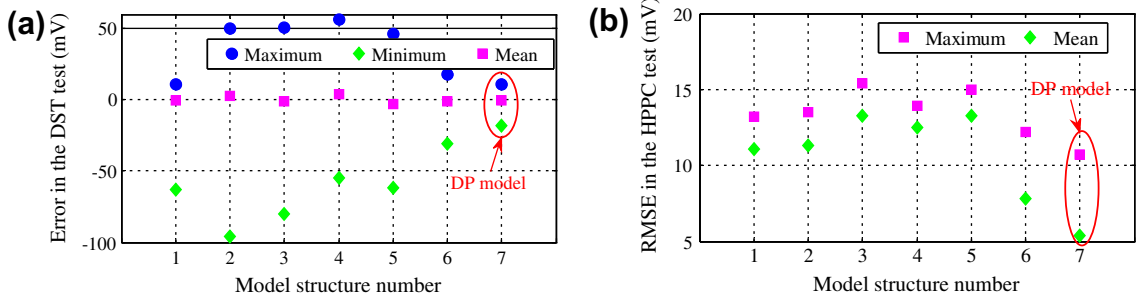

Fig. 8. Evaluation results under the DST test: (a) the statistics results of the voltage error and (b) the statistics results of the RMSE.

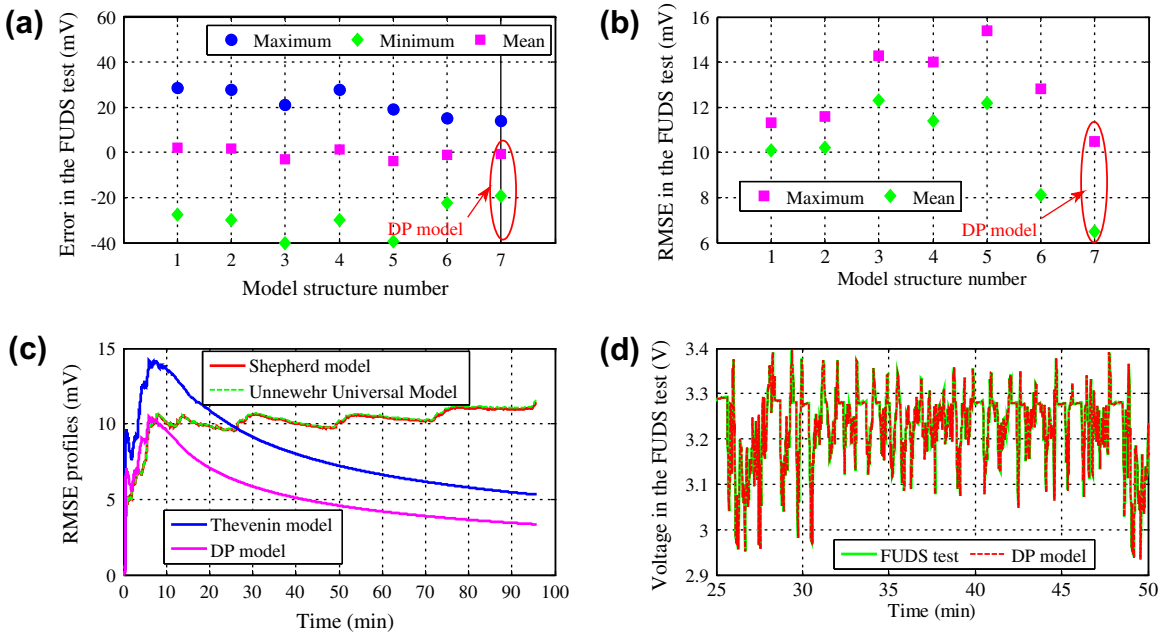

Fig. 10. Evaluation results under the FUDS test: (a) the statistics results of the voltage error; (b) the statistics results of the RMSE; (c) the RMSE profiles of four specific models; and (d) the voltage profiles of the *DP* model-based estimation and the FUDS test.

model is the second better model. Therefore, in the FUDS test, the *DP* model still has the most outstanding performance, followed by the *Thevenin* model; we can conclude that it is reasonable to refine the lithium-ion battery's voltage relaxation effect to improve the model-based estimated precision.

The evaluation results of the HPPC test, the DST test, the FUDS test come to one conclusion that the *Thevenin* model and the *DP* model are more accurate than the other five models owing to their considerations of the voltage relaxation effect to some extent. After refining the polarization characteristics, the accuracy of the *DP* model gets a significant improvement compared with the *Thevenin* model by connecting an additional RC network, does it mean that it will improve the model accuracy by connecting enough RC networks in series? We will discuss this next.

4.3. Discussions

The above evaluation results show that the equivalent circuit models considering the voltage relaxation effect have better performance than the other models, and the *DP* model with two RC networks has better dynamic voltage estimation precision than the *Thevenin* model with one RC network. In order to give a further study of the RC networks on the model accuracy, the battery general equivalent circuit model (GECM) with n RC networks is proposed as shown in Fig. 11.

Where C_i is the ith equivalent polarization capacitance and R_i is the ith equivalent polarization resistance simulating the transient response during a charge or discharge process, U_i is the voltage across C_i. $i = 1, 2, 3, 4, \ldots, n$.

The electrical behavior of the GECM model can be expressed by Eq. (11) in the frequency domain.

$$U_t(s) = U_{oc}(s) - I_L(s)\left(R_o + \frac{R_1}{1+R_1C_1s} + \cdots + \frac{R_n}{1+R_nC_ns}\right) \quad (n = 0, 1, 2, \ldots) \tag{11}$$

Similarly with the *Thevenin* model and the *DP* model, the GECM model can be discretized with the bilinear method [33], and then:

$$U_{t,k} = \left(1 - \sum_{i=1}^{n} c_i\right)U_{oc,k} + c_1U_{t,k-1} + c_2U_{t,k-2} + \cdots + c_nU_{t,k-n} + c_{n+1}I_{L,k} + c_{n+2}I_{L,k-1} + \cdots + c_{2n+1}I_{L,k-n} \tag{12}$$

where $c_i (i = 1, 2, \ldots, 2n+1)$ are the coefficient which contain model's parameters such as polarization capacitance, polarization resistance and open-circuit voltage

Define:

$$\begin{cases} \boldsymbol{\varphi}_{n,k} = [\,1 \quad U_{t,k-1} \quad U_{t,k-2} \quad \cdots \quad U_{t,k-n} \quad I_{L,k-1} \quad I_{L,k-2} \quad \cdots \quad I_{L,k-n}\,] \\ \boldsymbol{\theta}_{n,k} = \left[\left(1 - \sum_{i=1}^{n} c_i\right) \quad U_{oc,k} \quad c_1 \quad c_2 \quad c_3 \quad \cdots \quad c_{2n+1}\right]^T \end{cases} \tag{13}$$

Then the online parameters' identification matrix of the GECM model is built.

Considering the model complexity, when the number of the RC networks n is more than 5, a big error will arise from the linear discrete method. However, if other non-linear parameters' identification method is used such as the Kalman filters, there will cause a huge computing costs due to the complex model structure. So the evaluation tests are only conducted for the GECM models with $n = 1$–5 and the results are shown in Fig. 12.

Fig. 12 shows that for the HPPC test, the DST test and the FUDS test, the maximum of the absolute voltage errors is within 32 mV

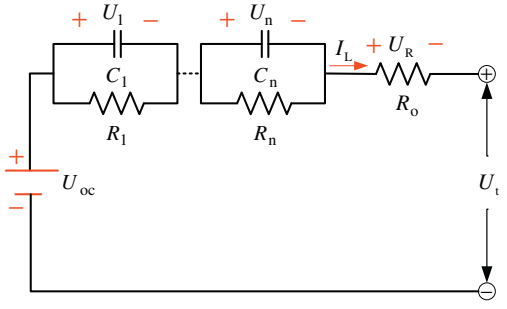

Fig. 11. The schematic diagram of the battery general equivalent circuit model.

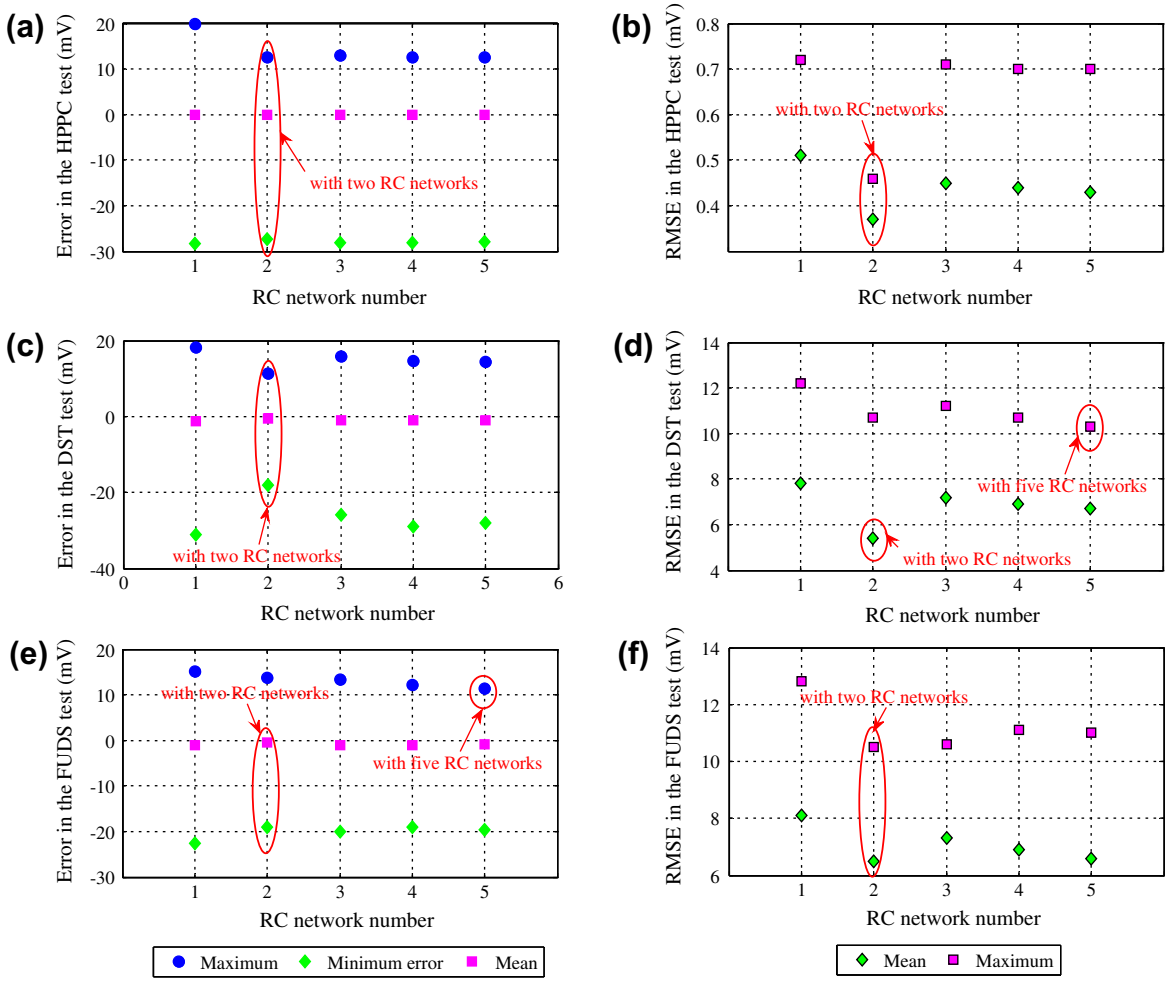

Fig. 12. Evaluation results of the GECM models: (a) the statistics results of the voltage error under the HPPC test; (b) the statistics results of the RMSE under the HPPC test; (c) the statistics results of the voltage error under the DST test; (d) the statistics results of the RMSE under the DST test; (e) the statistics results of the voltage error under the FUDS test; and (f) the statistics results of the RMSE under the FUDS test.

and the maximum of the RMSE is less than 15 mV. Fig. 12a shows that for the HPPC test, the GECM model with one RC network has the biggest voltage error, while the GECM model with two RC network performs best, but the mean of voltage error is not significant compared with the GECM model with three, four, five RC networks. Fig. 12b shows that the statistics of the RMSE are less than 1 mV, and the GECM model with two RC networks is the best. Fig. 12c shows that the GECM model with two RC networks has the smallest statistics values among the five models for the DST test; Fig. 12d shows the GECM model with two RC networks has the smallest mean of the RMSE while its maximum of the RMSE is bigger than the GECM model with five RC networks. However, the GECM model with two RC networks is simpler than that with five RC networks and is still the nest battery model after considering the practical applications.

Fig. 12e and f shows that for the FUDS test, the maximum of the voltage error of the GECM model with five RC networks performs better than the GECM model with two RC networks, However the GECM model with two RC networks performs the best in the absolute minimum, the mean of the voltage errors and statistics values of the RMSE. It can be concluded that the GECM model with two RC networks still shows the best performance.

In summary, the GECM model with two RC networks, also called the *DP* model, is the best model for the lithium-ion battery simulation. Further, it does not mean that the more RC networks the model has, the more accurate the model is. On the contrary, the performance of the GECM model with more than three RC networks becomes worse in some aspects.

5. Conclusion

This paper carries out a systematic evaluation on the seven typical battery models based on the HPPC test, DST test, FUDS test, and the GECM model with different RC networks is discussed further. Main conclusions are summarized as follows:

(1) The Seven commonly used battery models: *Shepherd* model, *Unnewehr Universal* model, *Nernst* model, *Combined* model, *Rint* model, *Thevenin* model, and the *DP* model are summarized, the model equations are deduced and the model parameters' identification method is designed based on the recursive least squares method with an optimal forgetting factor.

(2) The battery test bench is built and the experiment schedule is designed, which includes a characteristic test and an aging cycle test followed. The online identification process is conducted under the HPPC test, the DST test, the FUDS test for a $LiFeO_4$ lithium-ion battery.

(3) An evaluation method of the battery models is proposed and the evaluation results show that the voltage relaxation effect of the lithium-ion battery cannot be ignored, the *Thevenin*

model and the *DP* model both have good dynamic performance, and the *DP* model performs much batter for its more refined simulation of the voltage relaxation.

(4) A further discussion on the GECM model with different RC networks indicates that the GECM model with two RC networks, also called the *DP* model, is the best model for the lithium-ion battery simulation. The performance of the GECM model with more than three RC networks will become worse in some aspects.

We can conclude that the *DP* model shows the best performance among the seven commonly used models through our comprehensive comparison. The *DP* model performs the best in the DST test, which further proves that the *DP* model is suitable for the development of model-based BMS used in EVs.

Acknowledgements

This work was supported by the National High Technology Research and Development Program of China (2011AA112304, 2011AA11A228, 2011AA1290) in part, the International Cooperation Research Program of Chinese Ministry of Science and Technology (2010DFB 70090, 2011DFB70020) in part and also the research foundation of National Engineering Laboratory for Electric Vehicles in part. The author would also like to thank the reviewers for their corrections and helpful suggestions.

References

[1] Shuqin C, Nianping L, Jun G. Research on statistical methodology to investigate energy consumption in public buildings sector in China. Energy Convers Manage 2008;49:2152–9.
[2] Yao MF, Liu HF, Feng X. The development of low-carbon vehicles in China. Energy Policy 2011;39:5457–64.
[3] Titina B, Ferdinand T, Tomaž K. Energy conversion efficiency of hybrid electric heavy-duty vehicles operating according to diverse drive cycle. Energy Convers Manage 2009;50:2865–78.
[4] Brett W, Elliot M, Timothy L, Daniel K. Plug-in-hybrid vehicle use, energy consumption, and greenhouse emissions: an analysis of household vehicle placements in northern California. Energies 2011;4:435–57.
[5] Junping Wang, Jingang Guo, Lei Ding. An adaptive Kalman filtering based state of charge combined estimator for electric vehicle battery pack. Energy Convers Manage 2009;50(12):3182–6.
[6] He Hongwen, Xiong Rui, Chang Yuhua. Dynamic modeling and simulation on hybrid power system for electric vehicle application. Energies 2010;3:1821–30.
[7] Camus C, Farias T, Esteves J. Potential impacts assessment of plug-in electric vehicles on the Portuguese energy market. Energy Policy 2011;39:5883–97.
[8] Plett G. Extended Kalman filtering for battery management systems of LiPB-based HEV battery packs. Part 1. Background. J Power Sour 2004;134:252–61.
[9] Plett G. Extended Kalman filtering for battery management systems of LiPB-based HEV battery packs. Part 2. Modeling and identification. J Power Sour 2004;134:262–76.
[10] Plett G. Extended Kalman filtering for battery management systems of LiPB-based HEV battery packs. Part 3. State and parameter estimation. J Power Sour 2004;134:277–92.
[11] He Hongwen, Xiong Rui, Hongqiang Guo. Online estimation of model parameters and state-of-charge of $LiFePO_4$ batteries in electric vehicles. Appl Energy 2012;89:413–20.
[12] Piao CH, Fu WL, Lei GH, Cho CD. Online parameter estimation of the Ni-MH batteries based on statistical methods. Energies 2010;3:206–15.
[13] Yan J, Xu G, Qian H, Xu Y. Robust state of charge estimation for hybrid electric vehicles: framework and algorithms. Energies 2010;3:1654–72.
[14] Lee S, Kim J, Lee J, Cho BH. State-of-charge and capacity estimation of lithium-ion battery using a new open-circuit voltage versus state-of-charge. J Power Sour 2008;185:1367–73.
[15] He Hongwen, Xiong Rui, Fan Jinxin. Evaluation of lithium-ion battery equivalent circuit models for state of charge estimation by an experimental approach. Energies 2011;4:582–98.
[16] Vasebi A, Partovibakhsh M, Taghi Bathaee SM. A novel combined battery model for state-of-charge estimation in lead-acid batteries based on extended Kalman filter for hybrid electric vehicle applications. J Power Sour 2007;174:30–40.
[17] Zhu Wenhua H, Zhu Ying, Tatarchuk Bruce J. A simplified equivalent circuit model for simulation of Pb-acid batteries at load for energy storage application. Energy Convers Manage 2011;52(8–9):2794–9.
[18] Thermo Analytics: Battery Modeling for HEV Simulation by Thermo Analytics, Inc. <http://www.thermoanalytics.com/docs/batteries.html> [accessed 30.10.11].
[19] Hussein AA, Batarseh I. An overview of generic battery models. In: Proceedings of IEEE power and energy society general meeting, Detroit, MI, USA; 24–29 July, 2011.
[20] Hu XS, Li SB, Peng H. A comparative study of equivalent circuit models for Li-ion batteries. J Power Sour 2012;198(15):359–67.
[21] He Hongwen, Xiong Rui, Zhang Xiaowei, Sun Fenchun, Fan Jinxin. State-of-charge estimation of the lithium-ion battery using an adaptive extended Kalman filter based on an improved Thevenin model. IEEE Trans Veh Technol 2011;60:1461–9.
[22] Transportation Technology R&D Center. Argonne National Laboratory. <http://www.transportation.anl.gov/batteries/modeling_batteries.html> [accessed 30.10.11].
[23] Smith K, Rahn CD, Wang C. Model-based electrochemical estimation and constraint management for pulse operation of lithium ion batteries. IEEE Trans Control Syst Technol 2010;18:654–63.
[24] Chan HL. A new battery model for use with battery energy storage systems and electric vehicles power systems. In: Proceedings of IEEE symposium on power engineering society winter meeting, vol. 1; 2000. p. 470–5.
[25] Ziyad M, Margaret A, William A. A mathematical model for lead-acid batteries. IEEE Trans Energy Convers 1992;7:93–8.
[26] Goodwin GC, Sin KS. Adaptive filtering, prediction and control. Englewood Cliffs, NJ: Prentice-Hall; 1984.
[27] Jin J, Youmin Z. A revisit to block and recursive least squares for parameter estimation. Comput Electr Eng 2004;30(5):403–16.
[28] Ho YK, Farouq SM, Yeoh HK. Recursive least squares-based adaptive control of a biodiesel transesterification reactor. Indust Eng Chem Res 2010;49:11434–42.
[29] Fluke 8845A/8846A 6.5 digit Precision Multimeters. <http://www.fluke.com/fluke/uken/bench-instruments/bench-multimeters/8845a-8846a.htm?PID=55451>.
[30] Technical Specification of Battery Management System for Electric Vehicles. <www.catarc.org.cn/Upload/file/bzyj/PDF/zhengqiuyijian-sc27-19.pdf>.
[31] Idaho National Engineering & Environmental Laboratory. Battery test manual for plug-in hybrid electric vehicles; assistant secretary for energy efficiency and renewable energy (EE). Idaho Operations Office: Idaho Falls, ID, USA; 2010.
[32] Idaho National Engineering & Environmental Laboratory. Electric vehicle battery test procedures manual; assistant secretary for energy efficiency and renewable energy (EE). Idaho Operations Office: Idaho Falls, ID, USA; 1996.
[33] He Hongwen, Zhang Xiaowei, Xiong Rui, Yongli Xu, Guo Hongqiang. Online model-based estimation of state-of-charge and open-circuit voltage of lithium-ion batteries in electric vehicle. Energy 2012. http://dx.doi.org/10.1016/j.energy.2012.01.009.